Electronic Supplementary Material (ESI) for Nanoscale Advances.

Room-temperature magnetoresistance in $Ni_{78}Fe_{22}$/C8-BTBT/$Ni_{78}Fe_{22}$ nanojunctions fabricated from magnetic thin-film edges using a novel technique

---

Supplementary Information

Mizuki Matsuzaka[1], Yuma Sasaki[2], Kyohei Hayashi[1], Takahiro Misawa[2], Takashi Komine[3], Tomoyuki Akutagawa[4], Masaya Fujioka[2], Junji Nishii[2] and Hideo Kaiju[1,5]

[1]*Faculty of Science and Technology, Keio University, Yokohama, Kanagawa 223-8522, Japan*

[2]*Research Institute for Electronic Science, Hokkaido University, Sapporo, Hokkaido 001-0020, Japan*

[3]*Graduate School of Science and Engineering, Ibaraki University, Hitachi, Ibaraki 316-8511, Japan*

[4]*Institute of Multidisciplinary Research for Advanced Materials, Tohoku University, Sendai, Miyagi 980-8577, Japan*

[5]*Center for Spintronics Research Network, Keio University, Yokohama, Kanagawa 223-8522, Japan*

Correspondence and requests for materials should be addressed to H. K. (email: kaiju@appi.keio.ac.jp).

In this Supplementary Information section, we describe more detailed experimental methods and present some experimental results that were not included in the main text. In particular, we specify the polishing conditions, which were used to obtain the ultra-smooth surfaces of the glass/$Ni_{78}Fe_{22}$/glass substrates, and describe the OCSC fabrication process, which was utilized for the formation of C8-BTBT thin films on the polished surfaces of glass/$Ni_{78}Fe_{22}$/glass substrates. We also show the reproducibility of the fabrication method. In addition, we show AFM and c-AFM images of the polished glass/$Ni_{78}Fe_{22}$/glass surface with 2 nm thick C8-BTBT films, which are not shown in the main text, and the details of FT-IR study such as measurement conditions and FT-IR spectra of C8-BTBT. Moreover, we show the *I–V* curves in $Ni_{78}Fe_{22}$/$Ni_{78}Fe_{22}$ and $Ni_{78}Fe_{22}$ / C8-BTBT (2 or 4 nm) / $Ni_{78}Fe_{22}$ nanojunctions. Finally, we show the importance of the observation of positive MR, and additional experimental results of positive MR effect in $Ni_{78}Fe_{22}$ / C8-BTBT (4 nm) / $Ni_{78}Fe_{22}$ nanojunctions at different bias voltages.

Polishing conditions. Polishing of the cross-sectional surfaces of the glass/$Ni_{78}Fe_{22}$/glass substrates was conducted by utilizing two-step mechanical polishing (MP) and two-step chemical mechanical polishing (CMP) methods. The first MP process was performed on a cast-iron plate using Al_2O_3-based emeries (FUJIMI INCORPORATED, FO) in accordance with the following sequence of particle diameters: 93 (#240), 64 (#400), 46 (#600), and 18 (#1200) μm. The second MP process was performed on a polishing cloth (DP–DUR, Struers) using diamond pastes (DP–paste, Struers) with particle diameters of 3 and 1 μm in sequence. Afterwards, the first CMP treatment was performed on a polishing cloth (LAM PLAN, LAM 410) using Al_2O_3 slurries (Baikalox, Baikowski) with a particle diameter of 100 nm. The second CMP treatment was performed on a polishing cloth (DP–Chem, Struers) using colloidal SiO_2 slurries (OP–S, Struers) with a particle diameter of 40 nm. The second CMP process were conducted using a polishing machine (FACT–200, Nano Factor Co. LTD.) at a rotation speed of 60 rpm and room temperature.

OCSC fabrication process. Fig. S1(a) shows a schematic of OCSC process. The glass/$Ni_{78}Fe_{22}$/glass samples were placed away from the rotation axis of the spin coater at a distance of 2.5 cm. Fig. S1(b) shows a rotation speed during the OCSC process. The rotation speed increases with the time in the two-step manner.[1] Using the OCSC process, a uniform C8-BTBT layer can be deposited. C8-BTBT film with a thickness of more than 10 nm was obtained by 5 mg/ml solution in the original study,[1] while 2-nm-thick C8-BTBT films were obtained by 10 mg/ml solution in our study. The solution concentration is one of the factors that determine the film thickness. On the other hand, the film thickness also depends on the wettability between the molecules and the substrates when the films are deposited by spin-coating method, including OCSC method. Although the fabrication conditions were similar in both studies except for solution concentration, ITO-coated glass was used as a substrate in the original study, meanwhile the glass/$Ni_{78}Fe_{22}$/glass was used in our study. The use of different substrates could affect the variation of film thickness.

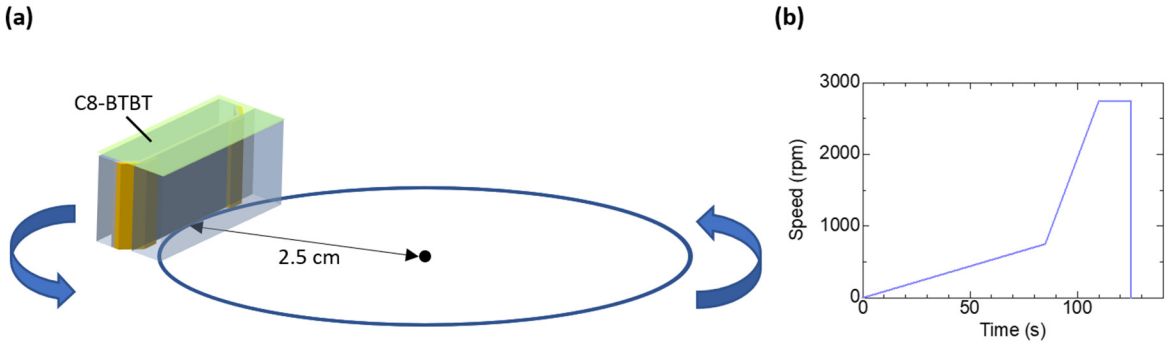

Fig. S1 (a) Schematic of OCSC process. The $Ni_{78}Fe_{22}$ film of the glass/$Ni_{78}Fe_{22}$/glass substrate was placed away from the center of the spin coater at a distance of 2.5 cm. (b) Rotation speed during the OCSC process.

Reproducibility of the fabrication method. Our proposed fabrication method consists of many processes. Here, we describe the reproducibility of the fabrication method. First, we can obtain the flat surface with a roughness of 0.6–0.8 nm as demonstrated in Fig. 3(c), the uniform electrical conduction along the $Ni_{78}Fe_{22}$ edges as illustrated in Fig. 3(d), and the ohmic *I–V* curves at an arbitrary position on the $Ni_{78}Fe_{22}$ edges as shown in Fig. 3(e) by the established polishing processes with good reproducibility. After the C8-BTBT films are deposited onto the polished surface, we can stack two electrodes. Since the nanometer-scale devices are sensitive to the mechanical vibration and static electricity, we should fix them carefully, after which the MR effect can be observed stably. When we stack the electrodes to fabricate $Ni_{78}Fe_{22}/Ni_{78}Fe_{22}$ nanojunctions in which two edges of $Ni_{78}Fe_{22}$ thin films are directly contacted, the electrical conduction can be easily obtained. The resistance of ~82 Ω can be obtained with excellent reproducibility in $Ni_{78}Fe_{22}/Ni_{78}Fe_{22}$ nanojunctions with a junction area of 42 × 42 nm^2. By contrast, in the nanojunctions sandwiching molecules, the more precise fixing process should be performed because the electric current does not flow easily through the molecular layer. Here, when the current was not able to flow in the devices, we can successfully obtain the electrical conduction in the device by repeating the polishing, spin-coating, and stacking processes (Fig. 2(f)–(h)). Moreover, a positive MR effect can be observed multiple times in $Ni_{78}Fe_{22}$ / C8-BTBT (4 nm) / $Ni_{78}Fe_{22}$ nanojunctions. In some cases, before the measurement of an MR effect, the device resistance decreases sharply to ~82 Ω due to the mechanical vibration when the device was moved into magnetic field in the air gap of the electromagnet. The device resistance of ~82 Ω implies that the short circuit is caused by the mechanical vibration. In this case, we fabricate the device again by repeating the above three processes (Fig. 2(f)–(h)). As a result, we can observe both *I–V* and MR curves.

Additional experimental results of AFM and c-AFM studies. Fig. S2 shows the AFM and c-AFM images of the polished glass/$Ni_{78}Fe_{22}$/glass surface covered with 2 nm thick C8-BTBT films.

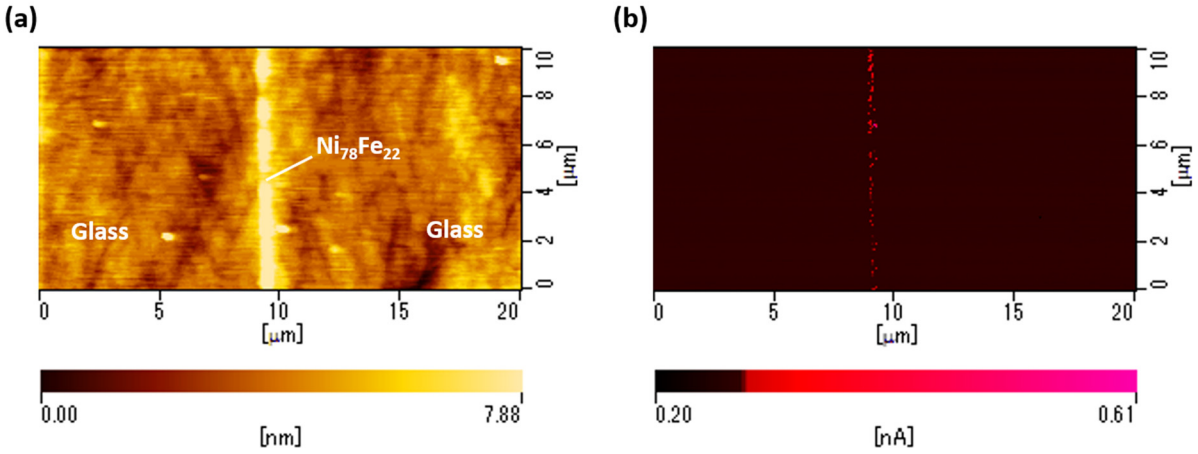

Fig. S2 (a) AFM and (b) c-AFM images of the polished glass / $Ni_{78}Fe_{22}$ (42 nm) / glass substrates coated with 2 nm thick C8-BTBT films.

FT-IR study of C8-BTBT. Fig. S3 shows the FT-IR spectra for C8-BTBT films measured by FT-IR (FT/IR-4X, JASCO Corporation). The spectra were obtained through reflection absorption spectroscopy (RAS). The wavelength of the ceramic light source ranges from 50 to 7800 cm^{-1}. Mercury cadmium telluride (MCT) is used for the photo detector. Clear IR spectra can be obtained for C8-BTBT thin films. The measured FT-IR spectra were in good agreement with the experimental reference data for C8-BTBT reported by other groups,[2–5] indicating the formation of high-quality C8-BTBT thin films.

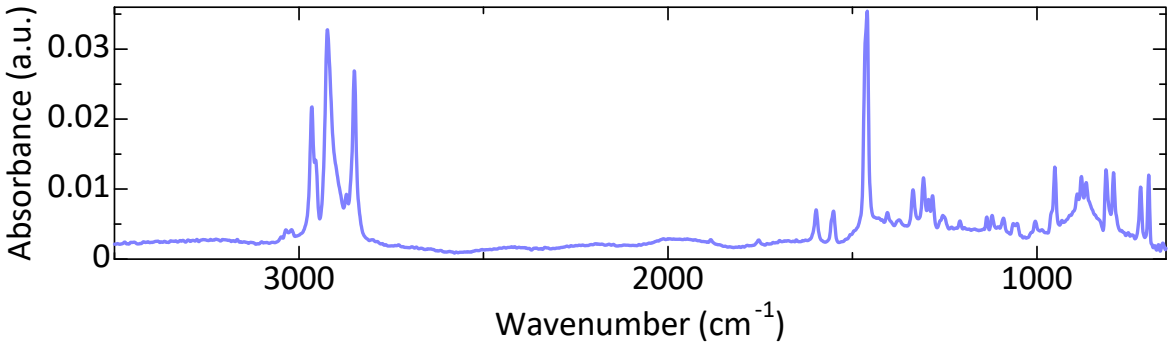

Fig. S3 FT-IR spectra for C8-BTBT thin films. The result agrees with the experimental reference data for C8-BTBT reported by other groups,[2–5] indicating the formation of high-quality C8-BTBT thin films.

***I–V* characteristics of nanojunctions.** Fig. S4 shows the *I–V* characteristics of $Ni_{78}Fe_{22}/Ni_{78}Fe_{22}$ and $Ni_{78}Fe_{22}$ / C8-BTBT (2 nm) / $Ni_{78}Fe_{22}$ nanojunctions, and Fig. S5 shows the *I–V* characteristics of $Ni_{78}Fe_{22}$ / C8-BTBT (4 nm) / $Ni_{78}Fe_{22}$ nanojunctions. The *I–V* curves were measured using a four-probe method at room temperature. Fig. S4(a), (b) and Fig. S5(a) were obtained in the same devices which exhibit the MR effect shown in Fig. 6(a), (b) and Fig. 7, respectively. Since the nanometer-scale devices are sensitive to the mechanical vibration and static electricity, when the device is moved into magnetic field in the air gap of the electromagnet, the resistance decreases due to the mechanical vibration. Therefore, the resistance (~186 Ω) shown in Fig. S5(a) is larger than the resistance (~160 Ω) which was obtained from MR effect shown in Fig. 7. Fig. S5(b) and (c) shows *I–V* curves obtained in $Ni_{78}Fe_{22}$ / C8-BTBT (4 nm) / $Ni_{78}Fe_{22}$ nanojunctions which are different from the device shown in Fig. S5(a). The resistance of the devices in Fig. S5 is within the range of 145.6–186 Ω, indicates that we can fabricate the nanojunctions with good reproducibility.

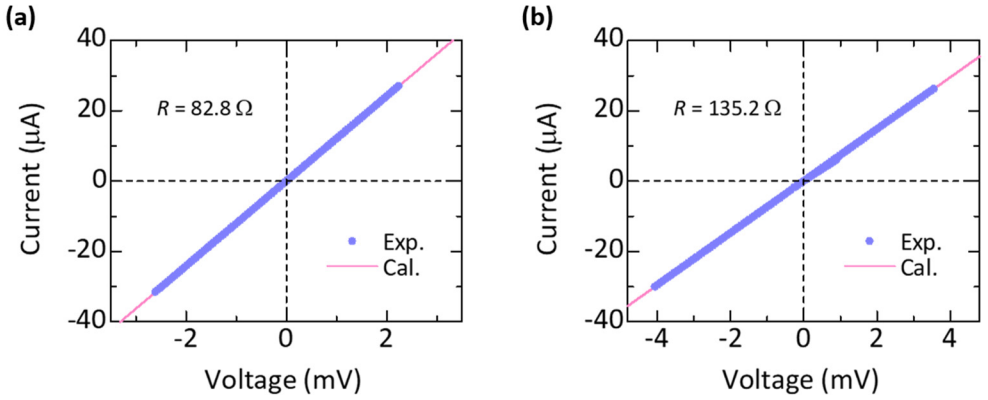

Fig. S4 *I–V* characteristics in (a) $Ni_{78}Fe_{22}/Ni_{78}Fe_{22}$ and (b) $Ni_{78}Fe_{22}$ / C8-BTBT (2 nm) / $Ni_{78}Fe_{22}$ nanojunctions with a junction area of 42 × 42 nm^2 at room temperature.

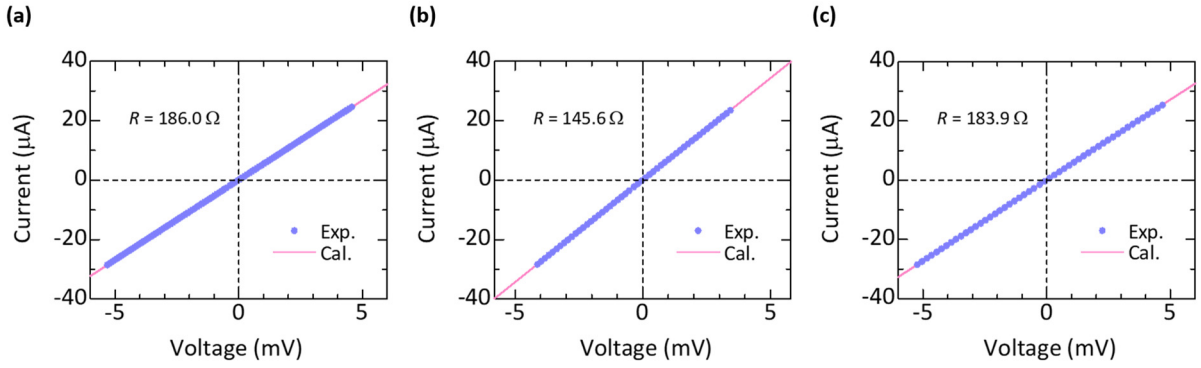

Fig. S5 *I–V* characteristics in $Ni_{78}Fe_{22}$ / C8-BTBT (4 nm) / $Ni_{78}Fe_{22}$ nanojunction with a junction area of 42 × 42 nm^2 at room temperature.

Positive MR effect. The positive MR effect is observed in $Ni_{78}Fe_{22}$ / C8-BTBT (4 nm) / $Ni_{78}Fe_{22}$ nanojunctions as shown in Fig. 7. The positive MR cannot be explained by AMR effect. The observation of the positive MR is also one of the evidence to rule out the possibility of electrode short circuit. These reasons are described here. AMR effect depends on the relative angle between the magnetization direction and current flow in the magnetic thin films. The resistance with a relative angle of 0° or 180° is higher than the resistance with a relative angle of 90°. In our study, when the magnetic field increases (decreases) from −190 (190) to 190 (−190) Oe, the relative angle changes from 180° (0°) to 0° (180°) (Fig. S6). When the magnetic field approaches the coercivity, the relative angle changes to 90°. Therefore, the resistance is high when the magnitude of magnetic field is large, meanwhile the resistance is low when the magnetic field is close to the coercivity. This means that the positive MR effect shown in Fig. 7 does not originate from AMR effect. Moreover, if a part of $Ni_{78}Fe_{22}$ thin-film edges sticks together, the electric current flows through the area of $Ni_{78}Fe_{22}/Ni_{78}Fe_{22}$, sandwiching no molecules. In this case, the observed MR effect is only AMR effect originating from $Ni_{78}Fe_{22}$ thin-film edges. Since the positive MR is observed as shown in Fig. 7, we can rule out the possibility of electrode short circuit.

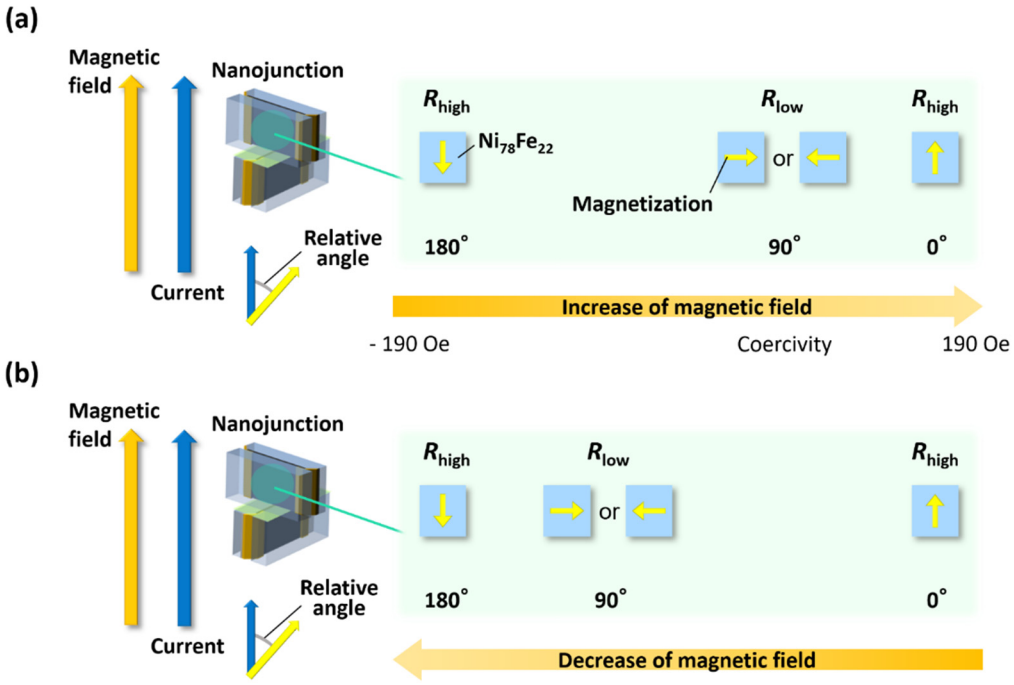

Fig. S6 Schematic illustration of AMR effect in this study during the (a) increase and (b) decrease of magnetic field.

Additional experimental results of positive MR effect. In the main text, a positive MR effect is shown in Fig. 7 at a bias voltage of 10.9 mV. Fig. S7 shows the MR effect in the $Ni_{78}Fe_{22}$ / C8-BTBT (4 nm) / $Ni_{78}Fe_{22}$ nanojunctions at different bias voltages of −14.9, −8.98, 8.34, and 9.20 mV. We can observe positive MR at various voltages. Fig. S8 shows a bias voltage dependence of the resistance. Here, $R_{P(AP)}$ is the resistance of parallel (anti-parallel) configuration of magnetization. The device resistance decreases with increasing the bias voltage, indicating that the current flows through C8-BTBT molecules. This behavior reveals that we have successfully observed a spin signal through the C8-BTBT molecules.

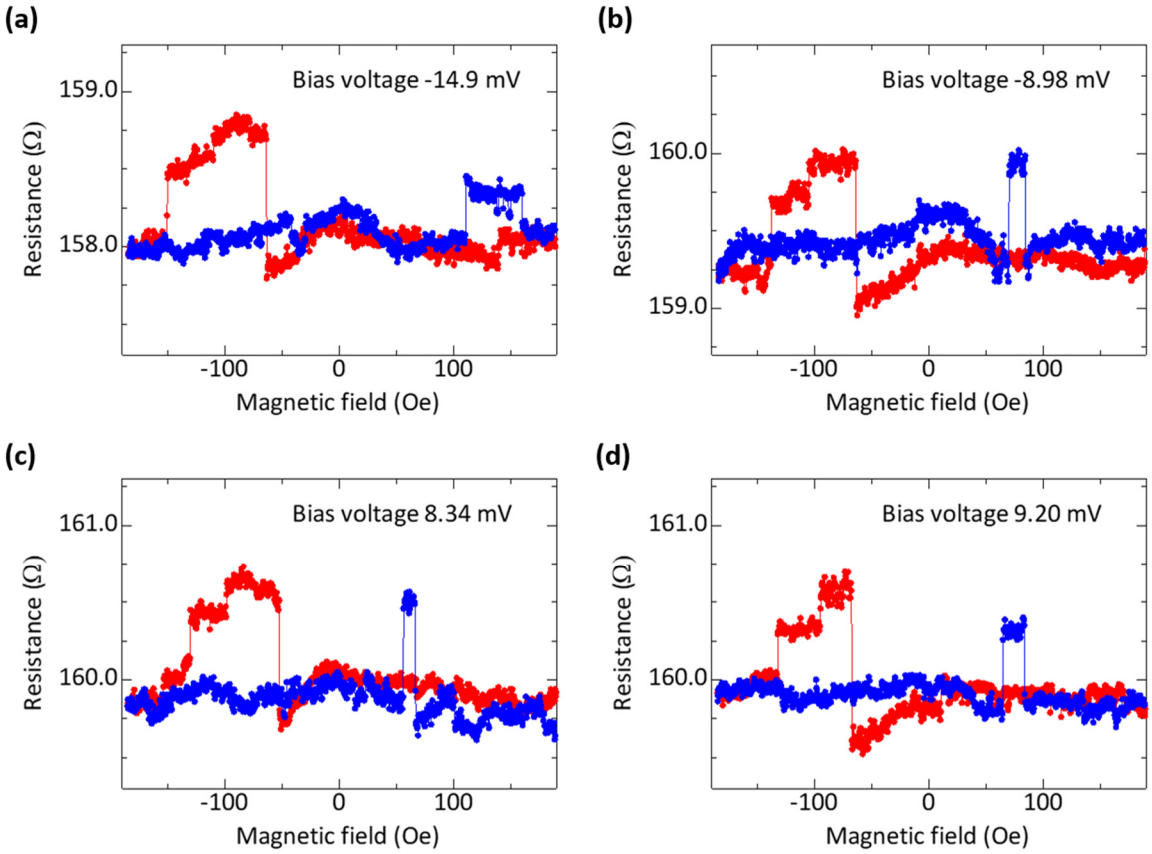

Fig. S7 MR effect in $Ni_{78}Fe_{22}$ / C8-BTBT (4 nm) / $Ni_{78}Fe_{22}$ nanojunction with a junction area of 42 × 42 nm^2 at room temperature. The bias voltage is (a) −14.9 mV, (b) −8.98 mV, (c) 8.34 mV and (d) 9.20 mV. We observe positive MR effects at each bias voltage.

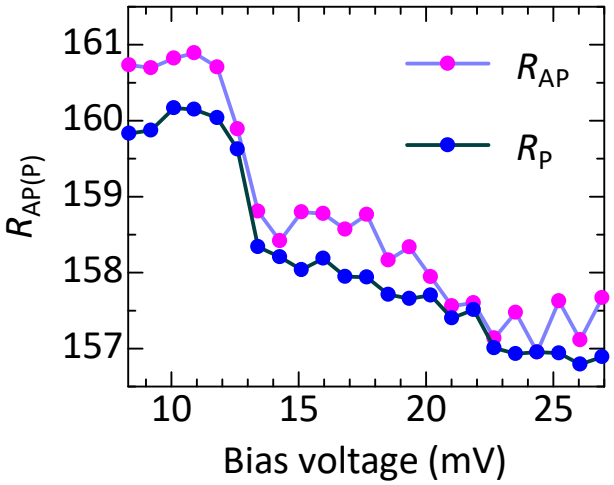

Fig. S8 Bias voltage dependence of the resistance in $Ni_{78}Fe_{22}$ / C8-BTBT (4 nm) / $Ni_{78}Fe_{22}$ nanojunctions.

References

1. Y. Yuan, G. Giri, A. L. Ayzner, A. P. Zoombelt, S. C. B. Mannsfeld, J. Chen, D. Nordlund, M. F. Toney, J. Huang and Z. Bao, *Nat. Commun.*, 2014, **5**, 3005.
2. Y. Li, C. Liu, M. V. Lee, Y. Xu, X. Wang, Y. Shi and K. Tsukagoshi, *J. Mater. Chem. C*, 2013, **1,** 1352–1358.
3. Y. Shibata, T. Matsuzaki, T. Ishinabe and H. Fujikake, *J. Cryst. Growth*, 2018, **492**, 98–104.
4. J. Mai, N. Tang, W. He, Z. Zou, C. Luo, A. Zhang, Z. Fan, S. Wu, M. Zeng, J. Gao, G. Zhou, X. Lu and J-M Liu, *Nanoscale Res. Lett.*, 2019, **14**, 169.
5. Z. Wang, H. Guo, J. Li, L. Wang and G. Dong, *Adv. Mater. Interfaces*, 2019, **6**, 1801736.